Differentiating between Primary Central Nervous System Lymphoma and Glioblastoma: The Diagnostic Value of Combining ¹⁸F-fluorodeoxyglucose Positron Emission Tomography with Arterial Spin Labeling

Junya HATAKEYAMA,[1] Takahiro ONO,[1] Masataka TAKAHASHI,[1]
Masaya ODA,[1] and Hiroaki SHIMIZU[1]

[1]Department of Neurosurgery, Akita University Graduate School of Medicine,
Akita, Akita, Japan

Abstract

Using conventional magnetic resonance imaging (MRI) methods, the differentiation of primary central nervous system lymphoma (PCNSL) and glioblastoma (GBM) is often difficult due to overlapping imaging characteristics. This study aimed to evaluate the diagnostic value of combining ¹⁸F-fluorodeoxyglucose positron emission tomography (FDG-PET) with arterial spin labeling (ASL) for differentiating PCNSL from GBM. In all, 20 patients with PCNSL and 55 with GBM were retrospectively examined. From the FDG-PET data, the maximum standardized uptake values (SUVmax) and the ratio of tumor to normal contralateral gray matter (T/N_SUVmax) were calculated. From the ASL data, the T/N ratio of the maximum tumor blood flow (relative TBFmax: rTBFmax) was obtained. Diagnostic performance of each parameter was analyzed using univariate and multivariate logistic regression analyses and receiver-operating characteristic (ROC) curve analyses. A generalized linear model was applied for comparing the performance of FDG-PET and ASL individually, and in combination. In univariate analysis, SUVmax and T/N_SUVmax were statistically higher in patients with PCNSL and rTBFmax was higher in patients with GBM. In the multivariate analysis, T/N_SUVmax and rTBFmax were statistically independent. The sensitivity, specificity, and area under the curve (AUC) for discriminating PCNSL from GBM were 100%, 87.3%, and 0.950 in T/N_SUVmax; 90%, 72.7%, and 0.824 in rTBFmax; and 95%, 96.4%, and 0.991 in the combined model, respectively. The combined use of T/N_SUVmax and rTBFmax may contribute to better differentiation between PCNSL and GBM.

Keywords: FDG-PET, arterial spin labeling, glioblastoma, primary central nervous system lymphoma, differentiation

Introduction

Primary central nervous system lymphoma (PCNSL) and glioblastoma (GBM) are two of the most common neoplasms found in the brain. They often appear similar on routine magnetic resonance imaging (MRI), but a precise differentiation is crucial because their managements are completely different. Chemotherapy and whole-brain radiotherapy, without extensive surgical resection, are the current treatment of choice for PCNSL.[1] In contrast, concurrent chemoradiotherapy after maximal surgical resection is the standard treatment for GBM.[2] Therefore, rapid and accurate differentiation is essential to improve the treatment outcome of patients with both PCNSL and GBM.

Several recent studies suggest that glucose metabolism by ¹⁸F-fluorodeoxyglucose positron emission tomography (FDG-PET)[3–9] may be useful for differentiating between PCNSL and GBM. Some studies also suggest the usefulness of perfusion-weighted MRI using gadolinium agents[10,11] or arterial spin labeling (ASL).[9,12–16] Both FDG-PET and ASL are less invasive and widely available; however, the

diagnostic efficacies of these methods are limited when applied individually.

The purpose of this study was to test our hypothesis that the combination of FDG-PET with ASL may improve the diagnostic accuracy for discriminating PCNSL from GBM.

Materials and Methods

This retrospective study was reviewed and approved by the institutional review board of our hospital. Written informed consent was obtained from all patients. The manuscript has been prepared according to the STARD statement.

Patients population and registration criteria

PCNSL and GBM patient data were extracted from our database. The inclusion criteria were as follows: (1) consecutive patients admitted to our hospital and diagnosed with PCNSL or GBM between October 2012 and June 2019; (2) diagnosis made by biopsy or surgical resection of the target lesion, and (3) both FDG-PET and MRI including ASL available prior to surgery. Histological diagnoses were made according to the World Health Organization classification.[17]

Patients with uncontrolled diabetes mellitus, acquired immune deficiency syndrome, or severe internal carotid artery stenosis, which may influence FDG-PET and/or ASL data, were excluded from the study. Steroid administration prior to imaging was allowed. In patients with GBM, immunohistochemical staining of IDH1 R132H was also tested.

[18]F-fluorodeoxyglucose positron emission tomography

A whole-body PET scanner (Headtome V, Shimadzu Co., Kyoto, Japan) or PET-computed tomography (PET-CT) scanner (Discovery ST Elite 16, GE Healthcare, Milwaukee, WI, USA) was used for PET data acquisition. Sixty minutes after intravenous administration of 185 MBq of ^{18}F-FDG (FDG Injectable; Nihon Medi-Physics, Tokyo, Japan), data were acquired in a three-dimensional (3D) fashion and 10 min/bed position with an axial field of view (FOV) of 30 cm in a 128×128 matrix. Plain 3D CT, the same FOV and matrix, was then obtained without moving the patient. Both FDG-PET and CT data were reconstructed with a slice thickness of 3.75 mm using VUE Point Plus; ordinary Poisson Ordered Subset Expectation Maximization with 10 subsets and two iterations were carried out.

Magnetic resonance imaging

All MRIs were obtained with 1.5-T (Signa HDxt; GE Healthcare) or 3.0-T unit (DISCOVERY MR750; GE Healthcare) MRI scanners with an 8- or 32-channel head coil. Imaging sequences included T2-weighted imaging (T2WI), T1-weighted imaging (T1WI), susceptibility-weighted imaging, contrast-enhanced T1WI (CE-T1WI), or 3D spoiled gradient-recalled (3D-SPGR) acquisition sequence with gadoteridol (ProHance, Esai, Tokyo, Japan), and ASL.

MRI parameters were as follows: spin-echo T1WI (TR 450-540; TE 8-10; flip angle 68–73°; matrix 320 × 256; FOV 22 cm; slice thickness 4 mm; slice gap 2 mm); fast spin-echo T2WI (TR 4025-5050; TE 99-130; flip angle 90–111°; matrix size 512 × 320; FOV 22 cm; slice thickness 4 mm; slice gap 2 mm); CE-T1WI (TR 400; TE 10; flip angle 3–90°; matrix 320 × 256; FOV 22 cm; slice thickness 4 mm; slice gap 2 mm); or 3D-SPGR (TR 5-10; flip angle 15°; matrix 256 × 192; FOV 22 cm; slice thickness 1.6 mm; slice gap 0.8 mm). A standard dose (0.2 mL/kg body weight) of gadoteridol was injected intravenously.

ASL was performed using a 3D fast spin-echo spiral sequence prepped with a pulsed-continuous ASL (TR 4600; TE 10.5; matrix 512 × 512; FOV 24 cm; slice thickness 4 mm; labeling pulse duration 1.5 sec; post-labeling delay 1525 msec). Pixel-based values reflecting cerebral blood flow (CBF; mL/100 g tissue/min) were provided by a preinstalled algorithm in the MRI unit.[18]

Image analysis

The FDG-PET and ASL data were analyzed using analytical software (SYNAPSE 5, Fujitsu Corporation, Tokyo, Japan) to obtain their values from region of interests (ROIs). In both FDG-PET and ASL images, the ROIs were manually placed in the enhancing area on CE-T1WI or 3D-SPGR, and values of FDG uptake or blood flow in the lesion without large vessels and hemorrhage were obtained (Fig. 1). If the lesion was in a central location, such as the corpus callosum or thalamus, the average value of both sides of normal gray matter was adopted as the reference. In the case of multiple tumors, the slice showing the maximum value was selected for the ROI analysis. When setting the ROIs of ASL, a point adjustment tool, preinstalled in SYNAPSE 5, was used because the angle of imaging plane of ASL was different from that of the contrast-enhanced images.

For FDG-PET image analysis, FDG uptake was calculated as the standardized uptake value (SUV) according to the following formula (constant factor = 10, calibration factor (CF) = 7.40×106): SUVmax = ROI (cps/g) × constant factor/injection dose (mCi) × body weight (g)/(cps/mCi). FDG uptake was represented as the pixel-based maximum SUV (SUVmax) within the ROIs covering the enhancing tumor.[3–6,9] The ratio of the SUVmax of the tumor to that of
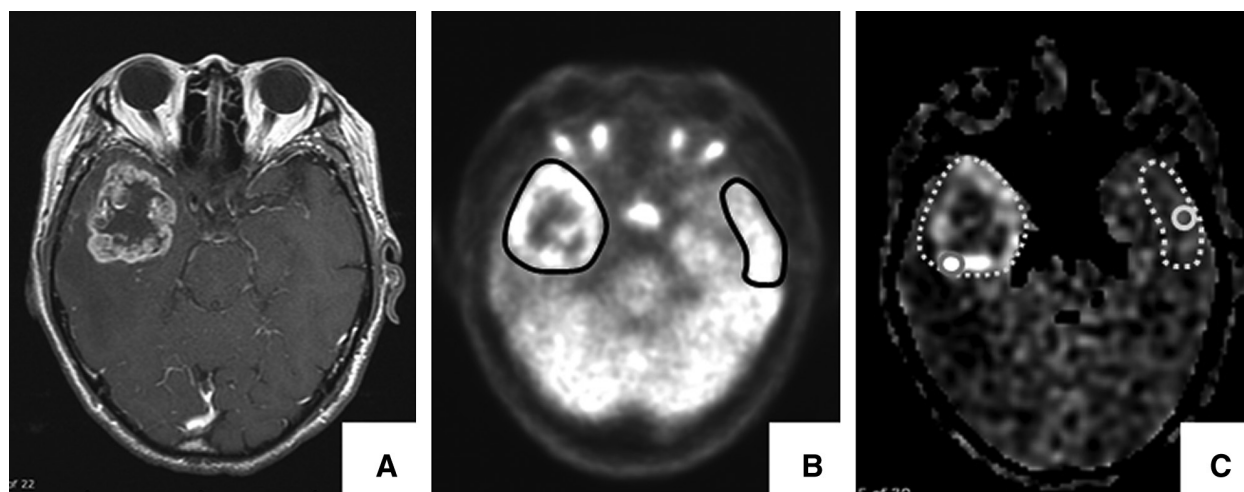
Fig. 1 **Representative images and the placement of ROIs for analyses a 79-year-old man, right temporal GBM.** (A) Contrast-enhanced T1WI showing enhanced lesions. (B) FDG-PET images showing the ROIs (black circles) for calculation of the pixel-based SUVmax in the lesion and contralateral reference. (C) ASL images showing increased intensities in the lesions. The aTBFmax and rTBFmax were calculated using a circular 10 mm² ROI (gray circles) placed in the most intense area within the enhancing lesion and contralateral reference (gray dot circles). ASL: arterial spin labeling, FDG-PET: ¹⁸F-fluorodeoxyglucose positron emission tomography, GBM: glioblastoma, ROIs: regions of interest, SUVmax: maximum standardized uptake values, aTBFmax: absolute maximum tumor blood flow, rTBFmax: relative maximum tumor blood flow.

the contralateral normal gray matter was generated as the T/N_SUVmax.

For ASL image analysis, an absolute maximum tumor blood flow (aTBFmax) and the maximum CBF of the contralateral normal gray matter were obtained based on a previous report.[16] Briefly, a circular 10 mm² ROI was placed in the most intense area of the tumor and contralateral normal gray matter on the same slice. The relative TBFmax (rTBFmax) was then generated by dividing aTBF by the maximum CBF. These parameters were compared if there were differences between 1.5-T and 3.0-T MRI units.

All procedures were independently performed by two of the authors (JH and TO), and averages of the two values were used for further analysis. JH and TO had full access to all raw clinical and image data and had final responsibility for the decision to submit for publication.

Statistical analysis

To evaluate the diagnostic significance and the statistical independence of each parameter, univariate and multivariate logistic regression analyses were performed. The sensitivity and specificity for discriminating PCNSL from GBM were calculated with the receiver-operating characteristics (ROC) analysis; the optimal cutoff point was the point showing the maximized sum of sensitivity and specificity. Area under the ROC curve (AUC) values

for the discrimination were calculated for each parameter. A generalized linear model was applied to compare the AUC of the diagnostic parameters individually, and in combination. P values less than 0.05 were considered statistically significant.

All statistical analyses were performed with EZR (Saitama Medical Center, Jichi Medical University, Saitama, Japan), which is a graphical user interface for R (The R Foundation for Statistical Computing, Vienna, Austria). More precisely, it is a modified version of the R commander designed to add statistical functions that are frequently used in biostatistics.[19]

Results

Participants

A total of 99 patients with GBM (n = 69) and PCNSL (n = 30) were admitted to our hospital and pathologically diagnosed between October 2012 and June 2019. Among them, 75 patients with GBM (n = 55) and PCNSL (n = 20) underwent both FDG-PET and ASL examinations before surgery and were registered in the present study. All GBMs were negative for IDH1 R132H and were presumed to be IDH wild type. All PCNSLs were diffuse large B-cell lymphomas, except for two cases of T-cell lymphoma.

The clinical characteristics of the present series are summarized in Table 1. There was no difference between GBM and PCNSL in terms of age and sex. Number of lesions on MRI was significantly more

in PCNSL than in GBM. Although both GBM and PCNSL were most frequently localized in the cerebral hemisphere, PCNSL often arose from the central structures such as the corpus callosum and thalamus. Owing to rapid clinical deterioration, 11 (20%) and 8 (40%) patients of GBM and PCNSL, respectively, were administered steroids before imaging studies. Regardless of the steroid administration, pathological diagnosis was possible in all cases.

Quantitative parameters and comparison of ASL data between 1.5-T and 3.0-T MRI units

The quantitative imaging parameters are also summarized in Table 1. Both SUVmax and T/N_SUVmax were significantly higher in patients with PCNSL, whereas both aTBFmax and rTBFmax were higher in GBM patients.

ASL data were obtained using 1.5-T MRI unit in 24 cases (17 GBM and 7 PCNSL), and 3.0-T in 51 cases (38 GBM and 13 PCNSL). The maximum CBF of the contralateral normal gray matter was significantly different between 1.5- and 3.0-T MRIs in both GBM and PCNSL groups, suggesting that aTBF max was also affected by the magnetic field strength as shown in Table 1. Therefore, we used rTBFmax (ratio of the aTBFmax and the corresponding contralateral CBF), which was not statistically different between 1.5- and 3.0-T MRIs in both GBM and PCNSL groups, as ASL data.

The effect of steroid administration

In patients with GBM, there was no significant difference in all quantitative parameters between the patients with and without steroid administration. Although SUVmax in PCNSL patients with steroid was higher than in those without (29.73 ± 8.31 vs. 23.14 ± 5.09, respectively, $p = 0.041$, t-test), there was no difference in T/N_SUVmax (2.98 ± 0.58 vs. 2.94 ± 0.69, respectively, $p = 0.90$). Also, steroid did not affect the value of rTBFmax in patients with PCNSL (1.37 ± 0.09 vs. 1.66 ± 0.54, respectively, $p = 0.15$).

Diagnostic significance

The diagnostic significance of SUVmax, T/N_SUVmax, and rTBFmax was analyzed using logistic regression analysis. The number of enhancing lesions that were significantly different between GBM and PCNSL patients was also included in the analysis (Table 2). The univariate analyses indicated that all parameters had statistical significance. The multivariate analyses demonstrated that T/N_SUVmax and rTBFmax were statistically significant and independent of each other.

Diagnostic performance of T/N_SUVmax and rTBFmax

The ROC analyses of each parameter and their combinations are shown in Fig. 2A. The combined use of T/N_SUVmax and rTBFmax (solid line, AUC = 0.991) showed the highest diagnostic performance compared to the T/N_SUVmax (middle broken line, AUC = 0.950) and rTBFmax (lower broken line, AUC = 0.824). Although AUCs of the combined model and rTBFmax were statistically significant ($p = 4.9 \times 10^{-4}$), there was no statistically significant difference between the combined model and T/N_SUVmax ($p = 0.077$).

A scatter diagram was generated using T/N_SUVmax and rTBFmax (Fig. 2B). Applying the cutoff points of each axis showing the maximum sum of sensitivity and specificity (2.07 for T/N_SUVmax and 2.23 for rTBFmax), discrimination between PCNSL from GBM was possible with 95% sensitivity and 96.4% specificity.

Figure 3 demonstrates the representative PCNSL and GBM cases that were difficult to distinguish by contrast-enhanced MRI alone but were possible by the combined use of FDG-PET and ASL. Three cases shown with the arrowheads and arrow in Fig. 2B were misdiagnosed by the current discrimination algorithm. These are cerebellar GBM with high Ki67 index (88%), temporal GBM with pleomorphic features, and histologically ordinary PCNSL.

Discussion

This study demonstrated the diagnostic accuracy of the combined use of FDG-PET and ASL for discriminating between PCNSL and GBM, with 95% sensitivity and 96.4% specificity. The AUC of the combined model was 0.991, which was superior to the values of each examination individually. Although various methods have been reported for the quantification of FDG-PET and ASL image data, we adopted the methods of measuring the maximum value of SUV in FDG-PET and TBF in ASL in the lesion and contralateral reference,[3–6,9,16] which is a simple and convenient technique.

Regarding FDG-PET, higher T/N_SUVmax values in PCNSL cases than in GBM coincided with the results of previous reports.[5–7,20,21] This may be accounted for by the higher cell density and/or higher glucose consumption rate of tumor cells in PCNSL.[5,6,20] The sensitivity and specificity of discriminating between the two tumors by FDG-PET alone have been reported to be 76.9–100% and 71.4–92.2%, respectively.[7–9,21] The present results of ASL, which showed lower rTBFmax in PCNSL cases, are also consistent with the results of previous studies.[9–11,14,16]

Table 1 Clinical characteristics and quantitative parameters of patients with GBM and PCNSL

Clinical characteristics	GBM (n = 55)	PCNSL (n = 20)	p value
Age at diagnosis, mean ± SD	66 ± 1.5	70 ± 8.7	0.34*
Sex, male/female	33/22	9/11	0.30**
Enhancing lesion in MRI, n (%)			
Single (%)	40 (73%)	10 (50%)	0.096**
Multiple (%)	15 (27%)	10 (50%)	
Number of lesions, mean ± SD	1.5 ± 1.1	2.3 ± 1.8	0.031*
Primary focus			
Cerebral hemisphere	49 (89.1%)	10 (50%)	
Supratentorial central structures	5 (9.1%)	7 (35%)	
Cerebellar hemisphere	0	2 (10%)	
Vermis	1 (1.8%)	1 (5%)	
Steroid administration prior to imaging	11 (20%)	8 (40%)	0.13**
Quantitative parameters, mean ± SD			
FDG-PET			
SUVmax	11.27 ± 4.21	25.78 ± 7.17	8.7×10^{-17}*
T/N_SUVmax	1.38 ± 0.63	2.95 ± 0.63	2.2×10^{-14}*
ASL			
Contralateral CBF	63.27 ± 17.24	65.11 ± 21.75	0.704*
1.5-T	70.71 ± 15.90 (n = 17)	83.97 ± 14.35 (n = 7)	
3.0-T	59.94 ± 16.95 (n = 38)	54.95 ± 18.07 (n = 13)	
p value (1.5-T vs. 3.0-T)	0.031*	0.018*	
aTBFmax	165.02 ± 79.87	96.38 ± 28.75	3.6×10^{-4}*
1.5-T	198.45 ± 113.63	110.00 ± 17.72	
3.0-T	150.06 ± 54.62	89.05 ± 31.39	
p value	0.037*	0.12*	
rTBFmax	2.71 ± 1.25	1.54 ± 0.44	1.1×10^{-4}*
1.5-T	2.89 ± 1.66	1.32 ± 0.17	
3.0-T	2.64 ± 1.03	1.66 ± 0.49	
p value	0.496*	0.097*	

*Student's t-test; **Fisher's exact test. ASL: arterial spin labeling, aTBFmax: absolute maximum tumor blood flow, CBF: cerebral blood flow, GBM: glioblastoma, MRI: magnetic resonance imaging, PCNSL: primary central nervous system lymphoma, rTBFmax: relative maximum tumor blood flow, SD: standard deviation, SUVmax: standardized uptake value, T/N: the ratio of tumor to normal contralateral gray matter.

This may reflect the blood–brain barrier destruction with neovascularization, which is commonly seen in GBM but rarely in PCNSL.[8,22,23] The reported sensitivity and specificity of ASL parameters for discrimination were 58.3–95.5% and 72.0–82.9%, respectively.[9,13,16]

In the present study, the absolute value of contra-lateral CBF and TBFmax obtained from 1.5-T MRI unit was higher than that obtained from 3.0-T unit. A previous study demonstrated the same tendency; there was machine-dependent difference in CBF measurement using ASL between 1.5-T and 3.0-T MRI unit.[24] The difference according to magnetic field strength should be noted; however, the cause is still unclear. Comparatively, You et al.[16] reported that the relative values of contralateral CBF and TBFmax were useful for differentiation between PCNSL and GBM, regardless of the magnetic field strength.[16] The present result is consistent with it, and supports the reliability of rTBFmax.

PCNSL cases with steroid administration showed higher SUVmax than that without. A previous study

Table 2 Parameters for discriminating between PCNSL and GBM

Univariate analysis	Odds ratio*	95% CI	p value
SUVmax	1.77	1.30–2.43	3.5×10^{-4}
T/N_SUVmax	18.1	4.87–67.6	1.6×10^{-5}
rTBFmax	0.17	0.059–0.47	7.7×10^{-4}
Number of enhancing lesions	1.46	1.01–2.13	0.047
Multivariate analysis			
T/N_SUVmax	261.0	3.23–21100	0.013
rTBFmax	0.0036	1.78×10^{-5}–0.72	0.018
Number of enhancing lesions	2.52	0.81–7.78	0.11

*Ratio for diagnosing PCNSL. CI: confidence interval, GBM: glioblastoma, PCNSL: primary central nervous system lymphoma, rTBFmax: relative maximum tumor blood flow, SUVmax: standardized uptake value, T/N: the ratio of tumor to normal contralateral gray matter.
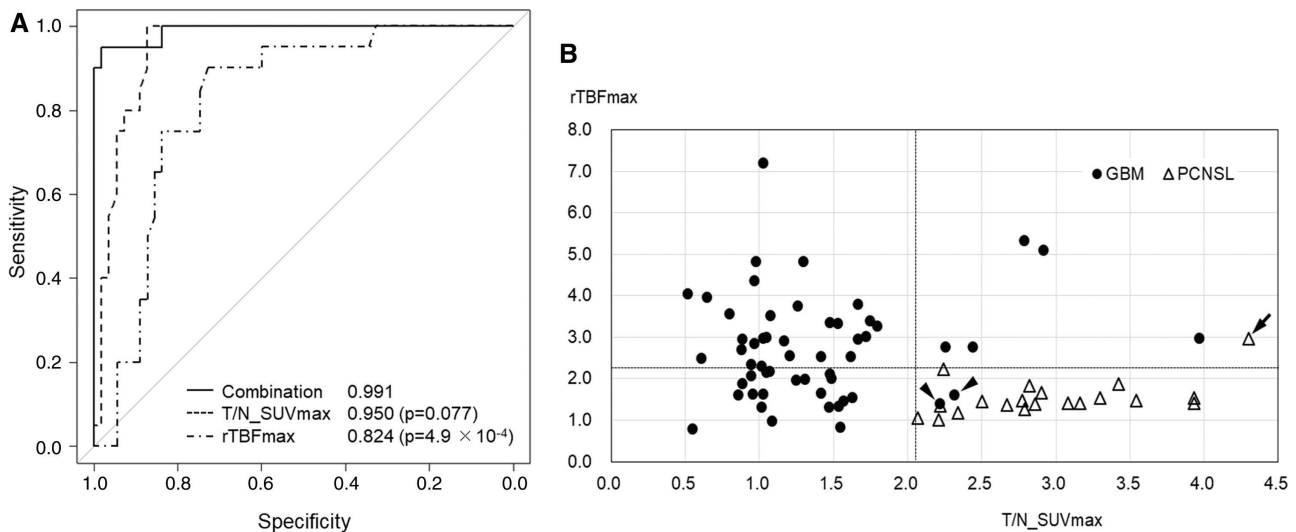
Fig. 2 (A) ROC curves generated using FDG-PET (middle broken line), ASL (lower broken line), and the combined use of two parameters according to generalized linear model (solid line). The AUC of the combined model (0.991) is higher than that of the T/N_SUVmax alone (0.950) and that of rTBFmax alone (0.824). And, the sensitivity and specificity discriminating PCNSL from GBM were 100% and 87.3% in T/N_SUVmax, 90% and 72.7% in rTBFmax, respectively. (B) A scatter diagram showing distribution along the rTBFmax (vertical) and T/N_SUVmax (horizontal) axes. The cutoff values of 2.23 for rTBFmax and 2.07 for T/N_SUVmax are shown with broken lines. The solid circles and open triangles depict GBM and PCNSL, respectively. Applying the cutoff points, the sensitivity and specificity for discrimination between PCNSL from GBM were 95% and 96.4%, respectively. One of the GBM cases (the left arrowhead) was the only case originating from the posterior fossa (the cerebellar vermis) in the present series. Histologically, this case included oligodendroglioma component and showed a high Ki67 index (88%). Another case with GBM of the right temporal lobe was that of a 22-year-old male patient (the right arrowhead), the youngest in the present series. Histological findings revealed a pleomorphic appearance, including giant and multinucleate cells with a high Ki67 index (41%). Despite their aggressive histological features, their clinical course was similar to the other cases with GBM. The misdiagnosed case of PCNSL (the arrow) showed high T/N_SUVmax and rTBFmax; however, its histological and clinical characteristics did not differ from that of the other PCNSL cases. AUC: area under the curve, FDG-PET: 18F-fluorodeoxyglucose positron emission tomography, GBM: glioblastoma, PCNSL: primary central nervous system lymphoma, ROC: receiver-operating characteristic, rTBFmax: relative maximum tumor blood flow, T/N_SUVmax: ratio of tumor to normal contralateral gray matter and maximum standardized uptake values.
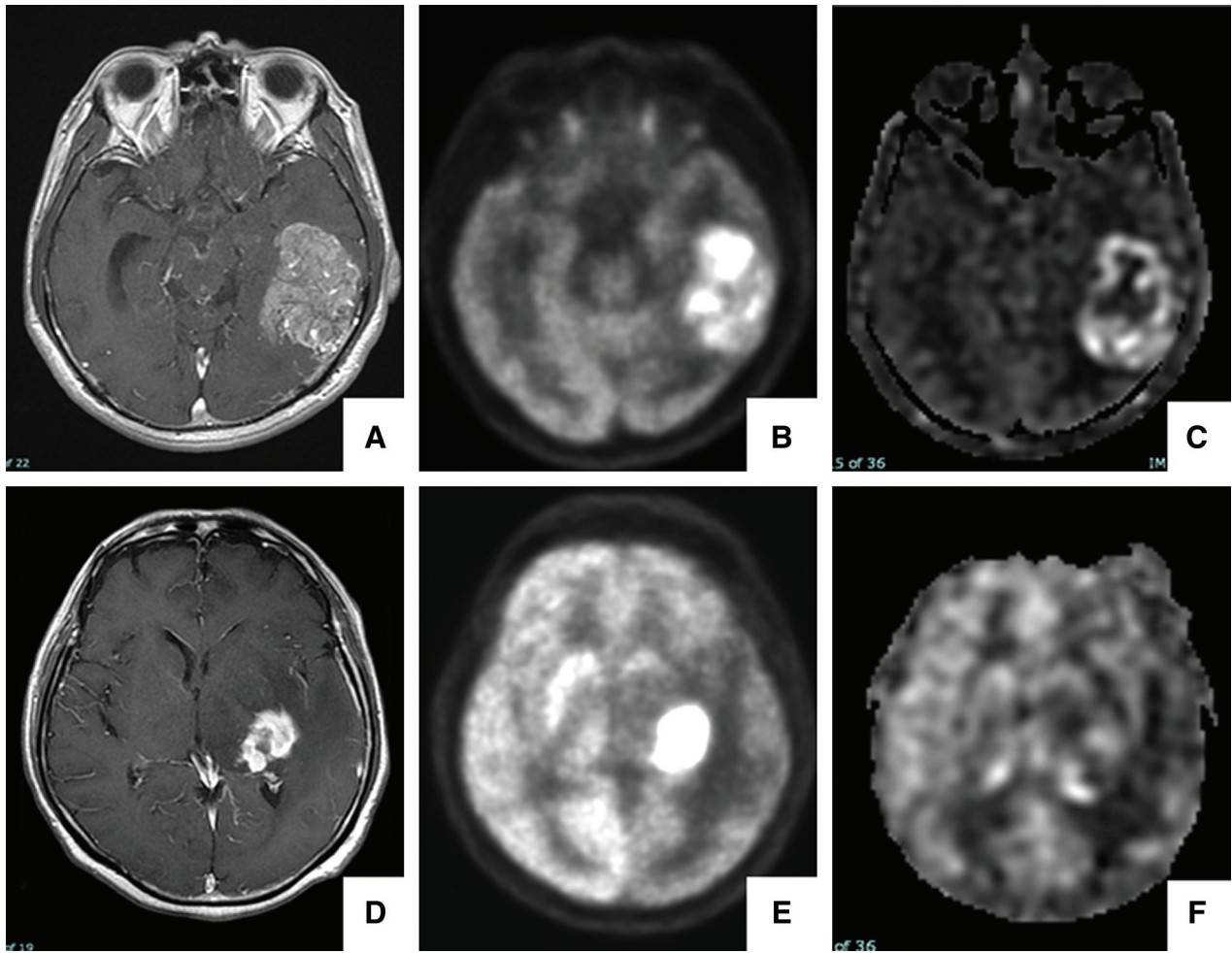
Fig. 3 The upper panel (A–C) shows a 58-year-old man with left temporal GBM. The patient presented with sensory aphasia and memory disturbance that had worsened over 1 week. (A) contrast-enhanced T1WI showing an enhancing lesion. (B) FDG-PET images showing partial high FDG accumulation (T/N_SUVmax: 2.79). (C) ASL images showing increased intensity in the lesion (rTBFmax: 5.53). Our scatter diagram suggested this case was a GBM, which was consistent with the histological diagnosis obtained by surgical resection. The lower panel (D–F) shows a 71-year-old man with PCNSL in the left basal ganglia. The patient presented with sensory aphasia and right hemiparesis that had worsened over 2 weeks. A level of soluble interleukin-2 receptor was 458 U/mL (normal range: 122–466). (D) Contrast-enhanced TIWI showing a heterogeneous enhancing lesion. (E) FDG-PET images showing marked FDG accumulation (T/N_SUVmax: 3.93). (F) ASL images showing slightly increased intensity in the lesion (rTBFmax: 1.42). Our scatter diagram suggested this case was a PCNSL, which was also consistent with the histological diagnosis obtained by stereotactic biopsy. ASL: arterial spin labeling, FDG-PET: ¹⁸F-fluorodeoxyglucose positron emission tomography, GBM: glioblastoma, PCNSL: primary central nervous system lymphoma, T1WI: T1-weighted images, T/N_SUVmax: ratio of tumor to normal contralateral gray matter and maximum standardized uptake values.

showed a negative correlation between SUVmax and steroid administration in PCNSL patients, which is not consistent with the present result.[7] Some reports demonstrate that PCNSL cases with high SUVmax show a poor clinical course.[25,26] Although not conclusive, the PCNSL cases in the present series requiring steroid administration might show rapid clinical and radiological progression; further study will be needed.

This study indicated a superior discriminating power of the combined use of FDG-PET with ASL. Although the AUC of the T/N_SUVmax did not differ statistically significantly from the combined use, AUC tended to be higher in the combined use. This is probably because of the independent and additive behavior of T/N_SUVmax and rTBFmax in diagnosis as shown in the multivariate analysis. Although contrast-enhanced perfusion MRI techniques are also reported

to be useful in this discrimination,[10,11] ASL would be superior in terms of less invasiveness.[10] FDG-PET is also less invasive and being widely performed for screening systemic malignancy including non-CNS lymphomas, metastatic brain tumors, and others.[27] Both PCNSL and GBM preferentially affect the elderly adult, and they often have various past medical histories and perioperative complications. The preoperative diagnosis using FDG-PET and ASL could justify a lesser invasive biopsy under local anesthesia for the patients with PCNSL, and aid in the discrimination when the contrast-enhanced MRI is contraindicated due to allergies or renal dysfunction.

However, the present discrimination algorithm also demonstrated its limitation. Two cases of GBM were missed because of relatively low rTBFmax as shown in Fig. 2B. These cases were different from other GBM cases in terms of the cerebellar origin in one, the younger age in the other, and the histological aggressiveness in both cases. This may be related to the findings that cerebellar GBM and adolescent GBM have molecular characteristics that are different from common GBMs.[28,29] *IDH 1/2* sequencing was not done in the present study. Although more than 90% of GBM showing IDH1 R132H-negative were IDH-wild-type GBM,[30] it cannot be denied that the present series included patients with rare *IDH* variants. Alternatively, the heterogeneous nature of TBF within GBMs may have been more problematic causing a partial volume effect on ASL rather than on PCNSLs, which would usually show a rather homogeneous and modest TBF.[8,9] This underestimation of TBF would likely occur in ring-enhancing GBMs.[9] Further studies will be necessary to elucidate what types of GBMs are likely to be exceptions of the present algorithm.

The PCNSL case that was misdiagnosed with the present algorithm showed a rather high rTBFmax and T/N_SUVmax without manifesting histological and clinical characteristics. The precise reason for this case is not clear and warrants further investigation.

Although the present discrimination strategy seems promising, it should be validated in other, preferably prospective cohorts, to prove the robust efficacy of this combinatorial algorithm.

In conclusion, the combined use of the T/N_SUVmax of FDG-PET and rTBF of ASL may be useful for preoperative differentiation between PCNSL and GBM with a sensitivity and specificity of 95% and 96.4%, respectively.

Acknowledgments

Conflicts of Interest Disclosure

All authors have no conflict of interest.

References

1) Ferreri AJ, Reni M: Primary central nervous system lymphoma. *Crit Rev Oncol Hematol* 63: 257–268, 2007

2) Stupp R, Mason WP, van den Bent MJ, et al.: Radiotherapy plus concomitant and adjuvant temozolomide for glioblastoma. *N Engl J Med* 352: 987–996, 2005

3) Albano D, Bosio G, Bertoli M, Giubbini R, Bertagna F: 18F-FDG PET/CT in primary brain lymphoma. *J Neurooncol* 136: 577–583, 2018

4) Kong Z, Jiang C, Zhu R, et al.: 18F-FDG-PET-based radiomics features to distinguish primary central nervous system lymphoma from glioblastoma. *Neuroimage Clin* 23: 101912, 2019

5) Kosaka N, Tsuchida T, Uematsu H, Kimura H, Okazawa H, Itoh H: 18F-FDG PET of common enhancing malignant brain tumors. *AJR Am J Roentgenol* 190: W365–369, 2008

6) Makino K, Hirai T, Nakamura H, et al.: Does adding FDG-PET to MRI improve the differentiation between primary cerebral lymphoma and glioblastoma? Observer performance study. *Ann Nucl Med* 25: 432–438, 2011

7) Yamaguchi S, Hirata K, Kobayashi H, et al.: The diagnostic role of 18F-FDG PET for primary central nervous system lymphoma. *Ann Nucl Med* 28: 603–609, 2014

8) Yamashita K, Hiwatashi A, Togao O, et al.: Diagnostic utility of intravoxel incoherent motion mr imaging in differentiating primary central nervous system lymphoma from glioblastoma multiforme. *J Magn Reson Imaging* 44: 1256–1261, 2016

9) Yamashita K, Yoshiura T, Hiwatashi A, et al.: Differentiating primary CNS lymphoma from glioblastoma multiforme: assessment using arterial spin labeling, diffusion-weighted imaging, and 18F-fluorodeoxyglucose positron emission tomography. *Neuroradiology* 55: 135–143, 2013

10) Järnum H, Steffensen EG, Knutsson L, et al.: Perfusion MRI of brain tumours: a comparative study of pseudo-continuous arterial spin labelling and dynamic susceptibility contrast imaging. *Neuroradiology* 52: 307–317, 2010

11) Makino K, Hirai T, Nakamura H, et al.: Differentiating between primary central nervous system lymphomas

and glioblastomas: combined use of perfusion-weighted and diffusion-weighted magnetic resonance imaging. *World Neurosurg* 112: e1–e6, Epub 2018 Feb 13

12) Chawla S, Wang S, Wolf RL, et al.: Arterial spin-labeling and MR spectroscopy in the differentiation of gliomas. *AJNR Am J Neuroradiol* 28: 1683–1689, 2007

13) Kim HS, Kim SY: A prospective study on the added value of pulsed arterial spin-labeling and apparent diffusion coefficients in the grading of gliomas. *AJNR Am J Neuroradiol* 28: 1693–1699, 2007

14) Noguchi T, Yoshiura T, Hiwatashi A, et al.: Perfusion imaging of brain tumors using arterial spin-labeling: correlation with histopathologic vascular density. *AJNR Am J Neuroradiol* 29: 688–693, 2008

15) Yoo RE, Choi SH, Cho HR, et al.: Tumor blood flow from arterial spin labeling perfusion MRI: a key parameter in distinguishing high-grade gliomas from primary cerebral lymphomas, and in predicting genetic biomarkers in high-grade gliomas. *J Magn Reson Imaging* 38: 852–860, 2013

16) You SH, Yun TJ, Choi HJ, et al.: Differentiation between primary CNS lymphoma and glioblastoma: qualitative and quantitative analysis using arterial spin labeling MR imaging. *Eur Radiol* 28: 3801–3810, 2018

17) Louis DOH, Wiestler OD, Cavenee WK: *World Health Organization classification of tumours of the Central Nervous System Revised 4th Edition.* Lyon, International Agency for Research on Cancer, 2016

18) GE Healthcare ed.: READY View User Guide 4th edition, Chapter 2: 58, 2015

19) Kanda Y: Investigation of the freely available easy-to-use software 'EZR' for medical statistics. *Bone Marrow Transplant* 48: 452–458, 2013

20) Herholz K, Pietrzyk U, Voges J, et al.: Correlation of glucose consumption and tumor cell density in astrocytomas. A stereotactic PET study. *J Neurosurg* 79: 853–858, 1993

21) Kawai N, Miyake K, Yamamoto Y, Nishiyama Y, Tamiya T: 18F-FDG PET in the diagnosis and treatment of primary central nervous system lymphoma. *Biomed Res Int* 2013: 247152, 2013

22) Calli C, Kitis O, Yunten N, Yurtseven T, Islekel S, Akalin T: Perfusion and diffusion MR imaging in enhancing malignant cerebral tumors. *Eur J Radiol* 58: 394–403, 2006

23) Kickingereder P, Sahm F, Wiestler B, et al.: Evaluation of microvascular permeability with dynamic contrast-enhanced MRI for the differentiation of primary CNS lymphoma and glioblastoma: radiologic-pathologic correlation. *AJNR Am J Neuroradiol* 35: 1503–1508, 2014

24) Tanaka Y, Inoue Y, Abe Y, Miyatake H, Hata H: Reliability of 3D arterial spin labeling MR perfusion measurements: the effects of imaging parameters, scanner model, and field strength. *Clin Imaging* 52: 23–27, 2018

25) Birsen R, Blanc E, Willems L, et al.: Prognostic value of early 18F-FDG PET scanning evaluation in immunocompetent primary CNS lymphoma patients. *Oncotarget* 9: 16822–16831, 2018

26) Kawai N, Zhen HN, Miyake K, Yamamaoto Y, Nishiyama Y, Tamiya T: Prognostic value of pretreatment 18F-FDG PET in patients with primary central nervous system lymphoma: SUV-based assessment. *J Neurooncol* 100: 225–232, 2010

27) Mohile NA, Deangelis LM, Abrey LE: The utility of body FDG PET in staging primary central nervous system lymphoma. *Neuro Oncol* 10: 223–228, 2008

28) Nomura M, Mukasa A, Nagae G, et al.: Distinct molecular profile of diffuse cerebellar gliomas. *Acta Neuropathol* 134: 941–956, 2017

29) Sturm D, Witt H, Hovestadt V, et al.: Hotspot mutations in H3F3A and IDH1 define distinct epigenetic and biological subgroups of glioblastoma. *Cancer Cell* 22: 425–437, 2012

30) Yan H, Parsons DW, Jin G, et al.: IDH1 and IDH2 mutations in gliomas. *N Engl J Med* 360: 765–773, 2009

Corresponding author: Takahiro Ono, MD, PhD
Department of Neurosurgery, Akita University Graduate School of Medicine 1-1-1, Hondo, Akita, Akita 010-8543, Japan.
e-mail: t.ono@med.akita-u.ac.jp